A short course of antibiotics selects for persistent resistance in the human gut

Eitan Yaffe[1,3]*, Les Dethlefsen[1], Arati V. Patankar[3], Chen Gui[3], Susan Holmes[4], David A. Relman[1,2,3]

[1]Department of Medicine, Stanford University School of Medicine, Stanford, CA USA.

[2]Department of Microbiology and Immunology, Stanford University School of Medicine, Stanford, CA USA.

[3]Infectious Diseases Section, Veteran Affairs Palo Alto Health Care System, Palo Alto, CA USA.

[4]Department of Statistics, Stanford University, Stanford, CA USA.

*Corresponding author. Email eitan.yaffe@stanford.edu

Understanding the relationship between antibiotic use and the evolution of antimicrobial resistance is vital for effective antibiotic stewardship, yet animal models and *in vitro* experiments poorly replicate real-world conditions. To elucidate how resistance evolves *in vivo*, we exposed 60 human subjects to ciprofloxacin and used longitudinal stool samples and a new computational method to assemble genomes for 5665 populations of commensal bacterial species within subjects. Analysis of 2.27M polymorphic sequence variants revealed 513 populations that underwent selective sweeps. We found convergent evolution focused on DNA gyrase and evidence of dispersed selective pressure at other genomic loci. Nearly 10% of susceptible bacterial populations evolved towards resistance through sweeps that involved mutations in a specific amino acid in gyrase. Evolution towards resistance was predicted by population abundances before and during the exposure. 89% of gyrase sweeps and the majority of all sweeps persisted more than 10 weeks. This work quantifies the direct relationship between antibiotic usage and the evolution of resistance within the gut communities of individual human hosts.

INTRODUCTION

Antimicrobial resistance (AMR) is a growing global health threat, projected to cause millions of deaths worldwide by 2050[1,2]. AMR is driven by the overuse and misuse of antibiotics[3], and is associated with geographic factors[4], seasonal patterns[5], and prolonged antibiotic usage[6]. AMR is not limited to heavily prescribed patients and is instead linked to low-intensity outpatient antibiotic usage[7]. Prescription data suggest that AMR primarily evolves due to bystander selective pressure, where colonizing pathogens evolve resistance subclinically in patients taking antibiotics for unrelated problems[8]. However, the evolution of AMR *in vivo* is rarely documented; instead, resistant pathogens usually emerge in infections after evolving elsewhere, as seen for example with resistant *Escherichia coli* associated with urinary tract infections[9] and surgical site infections[10]. In contrast to the sparsity of data from treated human subjects, the evolution of AMR has been extensively studied *in vitro*[11–17] and using animal models[18,19]. Yet, these laboratory experiments struggle to reproduce clinical conditions faithfully, most of which are poorly understood, including local drug concentrations that vary in time and space, microbial population sizes, the effects of immune system responses, and interactions within microbial communities[20–24]. Quantifying the evolution of AMR in clinically relevant settings can provide new opportunities for combatting AMR by informing antibiotic stewardship and developing personalized antibiotic treatments.

Fluoroquinolones are a class of potent broad-spectrum antibiotics that make up a fifth of global antibiotic consumption[25]. In contrast to the majority of antibiotics for which horizontal gene transfer plays an important role in the evolution of resistance[26,27], fluoroquinolone resistance (FQR) primarily involves mutations in the drug targets (Type II topoisomerases), with mobilized genes playing only a supporting role[28,29]. Analysis of pathogen genomes and *in vitro* experiments suggest that FQR evolves through a stepwise process that begins with specific mutations in DNA gyrase and topoisomerase IV[15,30–32]. However, the specific conditions under which these mutational processes occur in real-world settings remain poorly understood.

Commensal evolution in the gut of adults is evident over a timeframe of several years[33–36], and over shorter timeframes during the use of antibiotics[37], after fecal microbiota transplantation[38], or in newborns[39]. Fluoroquinolone concentrations in the human gut are high and persist days after oral treatment[40], exerting a strong selective pressure[41], and disrupting gut communities[42]. We therefore hypothesized that gut commensals would evolve resistance during a single, brief course of ciprofloxacin, allowing us to quantify key aspects of the evolution of AMR *in vivo*.

From a technical perspective, studying *in vivo* evolution in natural settings is challenging. The microbial communities within a single human gut are composed of hundreds of localized populations, each founded through one or several rounds of colonization[35,43]. Gene duplications and horizontal gene transfer result in a convoluted genomic landscape riddled with sequence homology between genomes, resulting in non-trivial relationships between genomes and genome assemblies[36]. One powerful genotyping approach is to sample a community repeatedly over time, which permits sequences to be associated and assembled based on their co-abundance across samples. Repeated sampling has been used to resolve genomes[44–46] and microbial strains[37,47–49]. However, existing strain recovery tools utilize heuristic approaches to identify true polymorphic sites, which are embedded in a background of spurious variant sites

that arise during genome assembly due to sequence homology within and between genomes. As of now, there is no method that effectively leverages dense longitudinal sampling to assemble genomes and accurately identify true polymorphic sites.

In this study, we exposed 60 subjects to a fluoroquinolone antibiotic, ciprofloxacin, orally for five days and collected longitudinal stool samples before and after exposure for a period of 20 weeks to study how gut commensals evolve under antibiotic selective pressure *in vivo*. To identify underlying polymorphisms, we developed a tool (PolyPanner) that simultaneously reconstructed 5665 genomes of localized populations of species and their 2.27M polymorphic variants. PolyPanner is unique in its ability to leverage the statistical power of longitudinal shotgun metagenomic data to address assembly errors and enrich for true polymorphic sites. Analysis of variants that swept in an antibiotic-associated manner uncovered evidence of convergent evolution focused on a pair of amino acids within the gene that encodes DNA gyrase subunit A, *gyrA*, alongside evidence of dispersed selective pressure elsewhere. Nearly 10% of susceptible microbial populations underwent sweeps in gyrA. The probability of a selective sweep was strongly influenced by population abundances both before and during antibiotic exposure. Finally, selective sweeps in *gyrA* and other genes persisted for months after the antibiotic exposure. This study provides valuable insights into the relationship between antibiotic usage and the evolution of resistance in human associated microbiotas.

RESULTS

Sixty healthy adult volunteers took a short course of ciprofloxacin (500mg orally, twice daily, 5 days) and self-collected 16 stool samples over a period of 20 weeks including daily sampling before, during and after the antibiotic exposure (960 samples in total, see **Supp. Fig. S1**). Stool-derived DNA libraries from all 960 samples were sequenced with 18.8M (million) reads per sample on average. We processed the temporal shotgun reads to generate metagenome-assembled genomes (MAGs) and their polymorphic sites using a workflow that combines standard metagenomic tools and PolyPanner, a program developed here and described in **Methods** (see **Supp. Fig. S2** for an overview of the workflow). Briefly, reads were pooled within subjects to generate 60 subject-specific metagenome co-assemblies spanning ~400Mb each on average. For each sample, reads were aligned to their respective subject assembly, generating single-nucleotide coverage profiles which represent fluctuations in the abundance of all assembled base pairs over the 16 time points. Chimeric contigs were segmented by applying an algorithm that located abrupt transitions in coverage profiles along contigs (**Methods**). These transitions are likely chimeric assembly breakpoints where the two sides of the breakpoint represent different populations. When applied to our dataset, the algorithm identified ~10k such breakpoints (involving 2.1% of contigs) per subject on average. Contigs were segmented on these breakpoints and the resulting segments were binned (i.e., clustered) based on average segment-level coverage profiles, resulting in 109k genome bins per subject on average. Downstream analysis was limited to 5665 MAGs (51-166 genomes per subject) that were at least 50% complete and not more than 10% contaminated. On average, the selected genomes were 81.3% complete and 1.8% contaminated (**Supp. Figure S3**), with median sequencing depth (summed across the 16 samples per subject) of 51x (5x to 3856x). Each genome putatively represented the

population of a single bacterial species inhabiting the gut of a specific subject. The 5655 populations spanned 924 distinct species, 378 genera and 81 families (**Supp. Table S1**).

Populations were disturbed yet mostly resilient to the antibiotic exposure

We examined the population-level response to the antibiotic exposure, as reflected by changes in population abundance over time. Population response trends included transient decreases and increases in abundance, indicating relative ciprofloxacin sensitivity and resistance or tolerance, as well as putative extinction events (**Fig. 1A**). During the height of the disturbance (days 3 to 8 after the start of ciprofloxacin) 15.9% of populations were below the detection limit and by the last sampling day (day 77) 9.7% of populations remained undetected and putatively extinct (**Fig. 1B**). Conversely, 0.9% of the populations were not observed at baseline and emerged during the height of the disturbance. The rank order of persistent populations was disrupted during the disturbance (Spearman rho=0.31) and returned closer to baseline by day 28 (rho=0.62). The relatively few extinction events and the overall return to baseline rank of persisting populations attested to the resilience of the human gut microbiome. Response trends were broadly associated with taxonomic identity (**Supp. Fig. S4**), yet diverse taxa such as the *Lachnospiraceae* family were highly heterogenous in their response (**Supp. Fig. S5**). The resilience of gut populations, despite the antibiotic-associated disruption, created a unique opportunity to assess how ciprofloxacin drives evolution in gut commensals.

Identifying polymorphic variants in mixed populations

We wished to identify true polymorphic sites, defined as variant sites that segregated within a single population. Mismatches in read alignments were identified on a single-nucleotide basis, resulting in variant sites typed as single nucleotide polymorphisms (SNPs), short insertions or deletions (indels), and genome rearrangement breakpoints. Sequencing errors were identified using a probabilistic approach and removed (**Methods**), resulting in 107.1 million variants. Due to genomic sequences shared between populations and duplicated genes within populations, not all variants inferred in this manner reflected true polymorphic variants (see illustration of concepts in **Supp. Fig. S6**). We developed a statistical approach to enrich for what we call *dynamic variants*, which are polymorphic variants with a non-constant frequency over time (**Methods**). The remaining variants, which we call *spurious variants*, reflect either homology between distinct populations (*ortholog variants*) or homology within a population due to duplicated genes (*paralog variants*). Spurious variants are considered noise for our purpose of tracking competing alleles within a single bacterial population. To our knowledge, this approach is the first explicit modelling and classification of variant types and allows one to enrich for true polymorphic variants using longitudinal shotgun data.

We assessed the density of spurious variants and benchmarked our ability to remove them by simulating data from 100 bacterial communities with different numbers of introduced dynamic variants (40G reads in total). In these simulated datasets, spurious variants were pervasive, with typically 50-150 spurious variants per Mb of genome, even when few mutations were simulated (**Supp. Fig. S7A**). With our approach, the fraction of spurious variants that were misclassified as

149 dynamic was less than 0.3%, regardless of sequencing depth, meaning that our approach
150 depleted the density of spurious variants by over 100-fold. Sensitivity depended on the
151 sequencing depth and the mutation type. Local mutations (SNPs and indels) began to be detected
152 at a sequencing coverage threshold of 50x per genome and plateaued at 60-80% of variants
153 detected (failing to reach 100% due to incomplete genome assemblies) when coverage was
154 above 100x (**Supp. Fig. S7B**). The sensitivity of detection for large-scale genome rearrangements
155 was lower (**Supp. Fig. S7C**). Importantly, the precision remained high in the face of "genetic
156 crowding" in which communities contained multiple members of the same genus or family (**Supp.
157 Fig. S8**). Taken together, simulated data demonstrated the pervasiveness of spurious variants
158 and showed that our approach is well-suited to detect dynamic variants in evolving bacterial
159 communities.

160

161 ***Hundreds of populations underwent putative selective sweeps***

162 Application of our approach to the 5665 populations detected 2.27 million dynamic variants,
163 making up 2.1% of all variants ("Genome" table in **Supp. Table S1**). Dynamic variants were
164 comprised of 98.5% SNPs, 1.3% indels and 0.2% rearrangement breakpoints. Dynamic variants
165 were found in 2133 populations (38%), and the percentage of populations with dynamic variants
166 among sufficiently sequenced populations (with an abundance above ~1%) was 85.8% (**Fig. 2A**).
167 We limited the analysis to 1866 populations that had 1-1000 dynamic variants, omitting 267
168 populations with over 1000 variants that were composed of distant conspecific strains.
169 Underlying strain genomes and their temporal trajectories were approximated using a
170 probabilistic model[48], resulting in 2-8 strains per population (**Fig. 2B**).

171 For each population, strains were arranged on a most-parsimonious phylogenetic tree, and each
172 tree branch was associated with a *linkage group* (LG), defined as the set of variants that were
173 inferred to change along the branch. We considered the LG size a crude estimator of the mean
174 age of the variants in the linkage group, where small linkage groups indicated recent events
175 (including *de novo* mutations and recombination events), and large groups earlier events. Smaller
176 LGs were correlated with elevated levels of non-synonymous mutations, measured using dN/dS
177 ratios (**Fig. 2C**).

178 There were 7132 variants that "swept" from a pre-antibiotic frequency below 20% to over 80%
179 post-antibiotic ("Variant" table in **Supp. Table S2**). Each sweeping variant represented a putative
180 mutation that transitioned from the baseline to the post-exposure variant state. Sweeping
181 variants involved 513 populations that were distributed across all subjects (8.55 ± 4.15
182 populations per subject) and involved 212 species (22.9% of species). Sweeping variants rarely
183 traveled alone: only 1% were the only member in their LG and 6.5% had 2-10 variants in their LG
184 (**Supp. Fig. S9**). We illustrate how variants are organized into strains and linkage groups using a
185 *Alistipes putredinis* population found in subject EBW, where an antibiotic-associated shift in
186 strain composition could be attributed to an LG composed of 2 mutations, one of which was in
187 the gyrase subunit A (*gyrA*) (**Fig. 2D**).
188

189 ***Convergent evolution focused on* gyrA**

190 A strain can sweep following antibiotic exposure because it carries an adaptive 'driver' mutation,
191 but additional 'passenger' variants in the same strain may also be swept to high abundance[50].
192 We therefore searched for evidence of evolution occurring in parallel in different populations
193 and subjects. To reduce the background noise of passenger variants, we focused our analysis
194 further on 1771 sweeping variants (in 312 populations) that were part of small LGs (up to 100
195 variants per LG). Variants were associated with single genes if intragenic or with two adjacent
196 genes if intergenic. Interestingly, 22.5% of implicated genes were associated with multiple
197 variants in the same population, indicating that at least some of the genetic variation was likely
198 introduced through recombination (**Supp. Fig. S10**).

199 Genes were annotated using the KEGG Orthology (KO) database, with special attention to
200 distinguishing between the homolog genes, gyrase subunit A (*gyrA*, K02469) and topoisomerase
201 IV subunit A (*parC*, K02621)[51,52] (**Supp. Fig. S11** and **Supp. Table S3**). Variants were assigned a
202 weight inverse to the size of their LG, and weights were aggregated within KOs, resulting in 803
203 KOs with positive weights. Weight enrichment ratios were computed over a background model
204 in which variants were randomly reassigned to a gene within their genome, resulting in 20
205 significant KOs that showed evidence of convergent evolution (**Supp. Fig. S12** and **Supp. Table**
206 **S4**). The top hit in terms of fold-enrichment and statistical significance was *gyrA* (68 variants, 373-
207 fold enrichment, $P < 1.25 \times 10^{-5}$) (**Fig. 2E**). *GyrA* sweeps occurred in 63 populations inhabiting
208 34 subjects. A dN/dS ratio of 3.9 and a median LG size of 2 were highly suggestive that *gyrA*
209 mutations occurred *de novo* within the gut of the subjects (**Fig. 2F**). See **Supp. Fig. S13** for
210 examples of *gyrA*-associated sweeps.

211 Beyond *gyrA*, the selective pressure was less focused and was distributed among the remaining
212 19 KOs, with no single KO involving more than 6 populations. Breakdown of KOs by taxonomic
213 identity showed how *gyrA* sweeps were widely distributed (41 species, 15 families), while other
214 KOs were typically limited to specific taxa (**Supp. Fig. S14**). Notably, *parC* was enriched in
215 mutations yet to a lesser degree (only 5 variants in 3 families) than its close homolog *gyrA*,
216 possibly because of reduced selective pressure due to its distinct role compared to DNA gyrase[53],
217 and in contrast to previous findings suggesting that Gram positive bacteria evolve primarily
218 through mutations in *parC*[28]. Other implicated KOs included efflux pumps (K02004), DNA
219 helicases (K02314, K03657), transport systems (K01537, K02051, K11085), transcription factors
220 (K19505) and phage-associated genes (K01421). The inhibition of the helicase DnaB (K02314) has
221 been implicated previously in FQR in *E. coli*[54]. While parallel evolution beyond *gyrA* was limited,
222 there were compelling examples of idiosyncratic sweeps that were not driven by *gyrA* (**Supp. Fig.**
223 **S15**).

224

225 ***Selective pressure targets specific amino acids within gyrA***

226 The mutations associated with *gyrA* were concentrated at two residues: *gyrA*:83 (56
227 substitutions) and *gyrA*:87 (9 substitutions) (*E. coli* numbering) (**Fig. 3A**). Substitutions at these
228 two positions are well-documented as initial steps towards fluoroquinolone resistance[29], and
229 accounted for 87% of *gyrA* substitutions observed in our study. We focused on *gyrA*:83

230 substitutions, which was by far the most common in our study, occurring in 33 subjects and in 38
231 species that spanned 11 taxonomic families. *GyrA*:83 substitutions were mainly serine to
232 phenylalanine (S83F, 21 cases) and serine to leucine (S83L, 19 cases) (**Fig. 3B**). To assess
233 substitution probabilities at position 83, we first resolved *gyrA*:83 at baseline for 3896 genomes
234 that contained *gyrA*. Serine, which is known to be associated with fluoroquinolone
235 susceptibility[15], was present at baseline in 61% of genomes, while leucine and phenylalanine,
236 associated with resistance, were present in 6% of the genomes (**Fig. 3C**). Baseline amino acids at
237 *gyrA*:83 were associated with taxonomic identity (**Supp. Fig. S16**). The probability of serine
238 substitution was 9.6±1.5% per population (**Fig. 3D**). In other words, nearly 10% of susceptible
239 bacterial populations evolved towards resistance *in vivo*. To our knowledge this is the first
240 estimation of the rate at which ciprofloxacin resistance evolves in human subjects.

241 Resistance mutations at *gyrA*:87 appeared less favorable. There were only 9 such instances, and
242 *Alistipes putredinis* accounted for five E87K mutations that likely occurred because these
243 genomes have an unusual initial serine codon at *gyrA*:83 (AGU) that would require two mutations
244 to reach the more favorable leucine or phenylalanine at position 83. Clinical isolates of *Neisseria*
245 *gonorrhoeae* were recently shown to gain resistance through mutations in *gyrA*:87, while keeping
246 serine at *gyrA*:83[55].

247

248 ***Evidence for pre-existing resistance***

249 We wished to leverage the large scope of the dataset to assess the prevalence of FQR prior to
250 ciprofloxacin exposure in our subjects. We determined species-specific resistance alleles at
251 *gyrA*:83 for 38 species, based on the identity of the substituting amino acid in sweeping variants.
252 Remarkably, resistance alleles were observed prior to the ciprofloxacin exposure in 26 of the 38
253 species (**Supp. Fig. S17**). For example, the resistance allele of *Phocaeicola vulgatus* was
254 phenylalanine (based on 2 sweeps with S83F), and there were 15 out of 34 populations with
255 phenylalanine at *gyrA*:83 before the exposure. Frequencies of resistant strains at baseline varied
256 among species, ranging between 0% to 71% and averaging 33.8% (**Fig. 3E**). Subjects did not have
257 significant differences in the overall level of pre-existing resistance, suggesting that most strains
258 were likely resistant prior to colonization, rather than evolving resistance *in situ* within subjects
259 (**Supp. Fig. S18**). Some species had a signature of pre-exposure resistance (based on
260 phenylalanine or leucine at *gyrA*:83), despite not having any observed sweeps in our study. For
261 example, the percentage of resistant *E. coli* strains was estimated to be 41% at baseline (based
262 on 5 leucines and 7 serines at *gyrA*:83), without any observed *gyrA* sweeps in *E. coli* populations.

263

264 ***Evolvability of resistance predicted by population size and drug sensitivity***

265 An important question with possible clinical implications is what determines the evolvability of a
266 population when challenged with ciprofloxacin, which is the probability that a population will
267 have one or more sweeping variants. For this analysis we focused on 410 populations (out of
268 5665) that had serine at *gyrA*:83 at baseline and had sufficient coverage for detection of sweeps,
269 if present (equivalent to an abundance over ~1%, as shown in Figure 2A). The overall evolvability
270 was 0.26 based on 106 populations with one or more sweep. *GyrA* evolvability (where at least

271 one sweep involves *gyrA*) was 0.11, based on 45 populations. Thus, *gyrA* evolution accounted for
272 only 36% of the overall evolvability, highlighting the putative role of alternative evolutionary
273 trajectories in response to antibiotics.

274 We employed logistic regression to assess whether abundance and taxonomic identity can serve
275 as reliable predictors for the *gyrA* evolvability of a population (**Sup. Figure S19**). Logistic
276 regression identified four significant predictors: baseline population abundance ($P<0.02$), the
277 decline in abundance during antibiotics (average of days 1-5, $P<10^{-5}$), and phylum (Bacteroidetes
278 $P<2x10^{-3}$ and Actinobacteria $P<2x10^{-8}$, relative to Firmicutes) (**Fig. 4A**). In terms of effect sizes,
279 *gyrA* evolvability exhibited a 3.8-fold increase for every 10-fold rise in baseline population
280 abundance and a 3.2-fold increase for every 10-fold rise in the magnitude of decline in abundance
281 during antibiotic exposure (i.e., the ratio between abundance at baseline and during treatment).
282 *GyrA* evolvability showed a strong association with drug sensitivity, as 90.2% of the populations
283 that underwent a *gyrA* sweep experienced a reduction in abundance during antibiotic exposure.
284 *GyrA* evolvability of Bacteroidetes and Actinobacteria was 3.8-fold and 26-fold higher than
285 Firmicutes, respectively. For the most susceptible populations (i.e., with a decline of 1000-fold or
286 more during antibiotics), evolvability equaled 0.5 when the baseline abundance was ~0.1% for
287 Bacteroides and ~1% for Firmicutes. Model-predicted evolvability and observed evolvability were
288 in agreement, when stratifying populations by baseline abundances (**Fig. 4B**), or by the decline in
289 abundance during antibiotics (**Fig. 4C**).

290 The model performance was excellent, with an area under the curve (AUC) of 0.875 (**Fig. 4D**). Of
291 note, a simple model that solely relies on the baseline abundance had an AUC of 0.76 and is
292 distinctive in its capability to predict evolvability using pre-exposure data. While differences in
293 genus-level *gyrA* evolvability were captured by the model in general, *Collinsella* (phylum
294 Actinobacteria) and *Lachnospira* (Firmicutes) were significantly more evolvable than predicted
295 by the model (**Fig. 4E**). Non-*gyrA* evolvability (i.e., the probability of a sweep with a gene other
296 than *gyrA*) was only partially explained by the abundance during antibiotics but not by the
297 abundance at baseline and was significantly harder to predict, reaching a maximal AUC of only
298 0.567 (**Supp. Fig. S20**). Evolvability was not significantly different between subjects (**Supp. Fig.
299 S21**).

300 The model parameters of *gyrA* evolvability are related to fundamental attributes of bacterial
301 populations: baseline abundances are linked to absolute population sizes and the magnitude of
302 the decline during antibiotics is a crude proxy for sensitivity to ciprofloxacin. The data and models
303 are consistent with an enrichment of *de novo gyrA* mutations that swept primarily in populations
304 that were both abundant and sensitive through a bottleneck event, while evolution through non-
305 *gyrA* variants had no clear signature of *de novo* mutations, likely drew from pre-existing standing
306 variation, and was not clearly associated with resistance.

307

308 ***Sweep reversion was slow***

309 Finally, we wanted to determine the long-term effect of the exposure, by examining sweep
310 reversions. At the time of the last sample, collected 10 weeks after the end of the exposure, 89%
311 of *gyrA* sweeps (65% of non-*gyrA* sweeps) remained at a frequency above 80% (**Fig. 5A**), and 74%

312 of *gyrA* sweeps (56% of non-*gyrA* sweeps) were at a frequency of 100% (**Fig. 5B**). To predict the
313 behavior beyond 10 weeks, we employed a naïve model that assumed a constant fitness cost for
314 resistant alleles, and separately inferred selection coefficients for all sweeps; see an example of
315 the fastest reverting *gyrA* sweep in **Fig. 5C**. Projecting one year out, 95% of *gyrA* sweeps were
316 not expected to fall below 1% frequency, which was higher than 84% for non-*gyrA* sweeps
317 (P<0.029, Yates's chi-squared test). The median reversion time for sweeps that were projected
318 to revert within a year was 109 days (**Fig. 5D**). Taken together, our data indicate that mutations
319 in *gyrA* and other loci can persist long after the antibiotic exposure, consistent with relatively low
320 fitness costs or compensatory mutations.

321

322 **DISCUSSION**

323 This work describes how gut commensals evolve *in vivo* during and after a single short course of
324 ciprofloxacin. We quantified, for the first time, rates at which AMR and other antibiotic-
325 associated mutations sweep and persist in human gut communities under clinically relevant
326 conditions. Our analysis shows that 11% of commensal populations acquire putative resistance
327 through mutations in *gyrA*, and over 80% of acquired genetic changes remain dominant months
328 after the antibiotic exposure. Evolvability through *gyrA* was explained by a simple model based
329 on population abundances, with marked differences between phyla. The study reveals key
330 factors that affect the evolution of ciprofloxacin resistance in humans.

331 Our data show that *gyrA* evolvability of bacterial populations surpasses a probability of 0.5 when
332 population abundances cross a threshold of 0.1% and 1%, for Bacteroides and Firmicutes
333 respectively, which together make up 86% of populations. Yet conservative assumptions result
334 in a theoretical upper bound for this threshold that ranges from 0.0002% to 0.002% (**Supp. Note**
335 **1**). The large discrepancy between theory and empirical data, and between phyla, may reflect
336 differences in mutation rates and sweep frequencies, and can also be explained by reduced
337 effective population sizes in the intestines due to flow[56]. Recent *in vitro* work with *E. coli*[15] and
338 *Pseudomonas aeruginosa*[16] showed that *gyrA* mutations sweep only when populations are large,
339 in agreement with our *in vivo* results. The emerging picture is that large populations can evolve
340 mutations in *gyrA* on their evolutionary trajectory towards higher levels of fluoroquinolone
341 resistance, while smaller populations may evolve through a variety of other mutations, if at all,
342 and are more likely to lose their resistance over time. From a clinical perspective, precise models
343 of evolvability can inform the selection of appropriate antibiotics, as previously suggested from
344 *in vitro* work[32]. To give a concrete example, a clinician treating a patient with a urinary tract
345 infection may decide against prescribing fluoroquinolones if sequencing data suggest that the
346 abundance of a gut-residing pathogen is high enough to predict evolution of resistance during
347 treatment. In the future, routine assessments of microbial composition and abundance could
348 become a useful tool for mitigating risk for the patient and society[3].

349 The method presented here exploits temporal shotgun metagenomic data, allowing us to re-
350 examine decades of *in vitro* studies and provide a more relevant understanding of how AMR
351 evolution transpires *in vivo*. The approach is well-suited to detect adaptive evolution in diverse
352 natural microbial communities facing selective pressure, although it has some limitations.
353 Studying horizontal gene transfer necessitates complementary methods like Hi-C[36,57] and long-

354 reads[37,58–60]. Additionally, the method is limited in its ability to detect 'soft' sweeps in which
355 multiple independent mutations sweep simultaneously[61]. Such phenomena, supported by *in vitro*
356 data, could play a significant role in the evolution of antimicrobial resistance[15].

357 The persistence of *gyrA* mutations may suggest that they have little or no fitness cost, a well-
358 known concern[28,62]. For example, *in vitro* experiments showed that replacing serine at *gyrA*:83
359 had no measurable fitness cost in *E. coli* and *Streptococcus pneumoniae*[63], or even conferred a
360 fitness advantage in pathogens such as *Salmonella* Typhi and *Campylobacter jejuni*[64,65]. For
361 mutations to revert, their fitness cost must supersede the nominal selective pressure in the gut
362 for a substantial length of time, yet the breadth of selective pressures under natural conditions
363 (other than antibiotics) remains poorly understood.

364 This approach can be used to understand the evolution of resistance *in vivo* with different
365 antibiotic classes, dosages, and durations, as well as previously unrecognized effects of other
366 drugs and conditions that impose selective pressure on the microbiome. The results of such
367 studies may inform the design of revised antibiotic regimens that better optimize benefit/cost
368 ratios[66,23]. By studying microbial communities in their natural environment, the net effect of
369 myriad interacting externalities on the evolution of community members can be distilled and
370 eventually understood.
371

372 **ACKNOWLEDGMENTS**

373 We extend our gratitude to Benjamin Good and Elizabeth Costello (Stanford University) for their
374 valuable insights and constructive feedback. This work was funded by the National Institute of
375 Allergy and Infectious Diseases of the National Institutes of Health grants R01AI147023 (DAR) and
376 R01AI112401 (DAR), and the Thomas C. and Joan M. Merigan Endowment at Stanford University
377 (DAR).

378

379 **AUTHOR CONTRIBUTIONS**

380 Conceptualization: EY, LD, DAR; Data Curation: EY, LD; Formal Analysis: EY; Investigation: AVP,
381 CG; Methodology: EY, SH; Software: EY; Supervision: EY, DAR; Validation: EY; Visualization: EY;
382 Writing – Original Draft Preparation: EY; Writing – Review & Editing: EY, LD, DAR.

383

384 **COMPETING INTERESTS**

385 The authors declare that they have no conflict of interest.

386

387 **DATA AVAILABILITY**

388 The source code for PolyPanner is available at https://github.com/eitanyaffe/PolyPanner.
389 Unprocessed DNA sequence reads are available in the NCBI database, under project
390 PRJNA974858.
391

392 **REFERENCES**
393

394 1. Harbarth, S. & Samore, M. H. Antimicrobial Resistance Determinants and Future Control.
395 *Emerg. Infect. Dis.* **11**, 794–801 (2005).
396 2. Murray, C. J. *et al.* Global burden of bacterial antimicrobial resistance in 2019: a systematic
397 analysis. *The Lancet* **399**, 629–655 (2022).
398 3. Lipsitch, M. & Samore, M. H. Antimicrobial Use and Antimicrobial Resistance: A Population
399 Perspective. *Emerg. Infect. Dis.* **8**, 347–354 (2002).
400 4. Goossens, H., Ferech, M., Vander Stichele, R. & Elseviers, M. Outpatient antibiotic use in
401 Europe and association with resistance: a cross-national database study. *The Lancet* **365**,
402 579–587 (2005).
403 5. Sun, D. S. *et al.* Analysis of multiple bacterial species and antibiotic classes reveals large
404 variation in the association between seasonal antibiotic use and resistance. *PLoS Biol.* **20**,
405 e3001579 (2022).
406 6. Marvig, R. L., Sommer, L. M., Jelsbak, L., Molin, S. & Johansen, H. K. Evolutionary insight from
407 whole-genome sequencing of *Pseudomonas aeruginosa* from cystic fibrosis patients. *Future*
408 *Microbiol.* **10**, 599–611 (2015).
409 7. Olesen, S. W. *et al.* The distribution of antibiotic use and its association with antibiotic
410 resistance. *eLife* **7**, e39435 (2018).
411 8. Tedijanto, C., Olesen, S. W., Grad, Y. H. & Lipsitch, M. Estimating the proportion of bystander
412 selection for antibiotic resistance among potentially pathogenic bacterial flora. *Proc. Natl.*
413 *Acad. Sci.* **115**, E11988–E11995 (2018).
414 9. Stracy, M. *et al.* Minimizing treatment-induced emergence of antibiotic resistance in
415 bacterial infections. *Science* **375**, 889–894 (2022).
416 10. Long, D. R. *et al.* 2021 Young Investigator Award Winner: Anatomic Gradients in the
417 Microbiology of Spinal Fusion Surgical Site Infection and Resistance to Surgical
418 Antimicrobial Prophylaxis. *Spine* **46**, 143–151 (2021).
419 11. Hegreness, M., Shoresh, N., Damian, D., Hartl, D. & Kishony, R. Accelerated evolution of
420 resistance in multidrug environments. *Proc. Natl. Acad. Sci.* **105**, 13977–13981 (2008).
421 12. Toprak, E. *et al.* Evolutionary paths to antibiotic resistance under dynamically sustained
422 drug selection. *Nat. Genet.* **44**, 101–105 (2012).
423 13. Lázár, V. *et al.* Bacterial evolution of antibiotic hypersensitivity. *Mol. Syst. Biol.* **9**, 700
424 (2013).
425 14. Rodriguez de Evgrafov, M., Gumpert, H., Munck, C., Thomsen, T. T. & Sommer, M. O. A.
426 Collateral Resistance and Sensitivity Modulate Evolution of High-Level Resistance to Drug
427 Combination Treatment in *Staphylococcus aureus*. *Mol. Biol. Evol.* **32**, 1175–1185 (2015).
428 15. Garoff, L. *et al.* Population Bottlenecks Strongly Influence the Evolutionary Trajectory to
429 Fluoroquinolone Resistance in *Escherichia coli*. *Mol. Biol. Evol.* **37**, 1637–1646 (2020).
430 16. Mahrt, N. *et al.* Bottleneck size and selection level reproducibly impact evolution of
431 antibiotic resistance. *Nat. Ecol. Evol.* **5**, 1233–1242 (2021).
432 17. Lopatkin, A. J. *et al.* Clinically relevant mutations in core metabolic genes confer antibiotic
433 resistance. *Science* **371**, eaba0862 (2021).

434 18. Münch, P. C. *et al.* Pulsed antibiotic treatments of gnotobiotic mice manifest in complex
435 bacterial community dynamics and resistance effects. *Cell Host Microbe* **31**, 1007-1020.e4
436 (2023).
437 19. Vasquez, K. S. *et al.* Quantifying rapid bacterial evolution and transmission within the
438 mouse intestine. *Cell Host Microbe* **29**, 1454-1468.e4 (2021).
439 20. Fung-Tomc, J. C. Correlation of in vitro and in vivo resistance development to antimicrobial
440 agents. *Antimicrob. Newsl.* **7**, 17–24 (1990).
441 21. Hughes, D. & Andersson, D. I. Evolutionary Trajectories to Antibiotic Resistance. *Annu. Rev.*
442 *Microbiol.* **71**, 579–596 (2017).
443 22. Jahn, L. J., Munck, C., Ellabaan, M. M. H. & Sommer, M. O. A. Adaptive Laboratory Evolution
444 of Antibiotic Resistance Using Different Selection Regimes Lead to Similar Phenotypes and
445 Genotypes. *Front. Microbiol.* **8**, 816 (2017).
446 23. Relman, D. A. & Lipsitch, M. Microbiome as a tool and a target in the effort to address
447 antimicrobial resistance. *Proc. Natl. Acad. Sci.* **115**, 12902–12910 (2018).
448 24. Bottery, M. J., Pitchford, J. W. & Friman, V.-P. Ecology and evolution of antimicrobial
449 resistance in bacterial communities. *ISME J.* **15**, 939–948 (2021).
450 25. Browne, A. J. *et al.* Global antibiotic consumption and usage in humans, 2000–18: a spatial
451 modelling study. *Lancet Planet. Health* **5**, e893–e904 (2021).
452 26. Moradigaravand, D. *et al.* Prediction of antibiotic resistance in Escherichia coli from large-
453 scale pan-genome data. *PLoS Comput. Biol.* **14**, e1006258 (2018).
454 27. Hicks, A. L. *et al.* Evaluation of parameters affecting performance and reliability of machine
455 learning-based antibiotic susceptibility testing from whole genome sequencing data. *PLoS*
456 *Comput. Biol.* **15**, e1007349 (2019).
457 28. Redgrave, L. S., Sutton, S. B., Webber, M. A. & Piddock, L. J. V. Fluoroquinolone resistance:
458 mechanisms, impact on bacteria, and role in evolutionary success. *Trends Microbiol.* **22**,
459 438–445 (2014).
460 29. Bush, N. G., Diez-Santos, I., Abbott, L. R. & Maxwell, A. Quinolones: Mechanism, Lethality
461 and Their Contributions to Antibiotic Resistance. *Molecules* **25**, 5662 (2020).
462 30. Li, X., Mariano, N., Rahal, J. J., Urban, C. M. & Drlica, K. Quinolone-Resistant *Haemophilus*
463 *influenzae* : Determination of Mutant Selection Window for Ciprofloxacin, Garenoxacin,
464 Levofloxacin, and Moxifloxacin. *Antimicrob. Agents Chemother.* **48**, 4460–4462 (2004).
465 31. Morgan-Linnell, S. K. & Zechiedrich, L. Contributions of the Combined Effects of
466 Topoisomerase Mutations toward Fluoroquinolone Resistance in *Escherichia coli*.
467 *Antimicrob. Agents Chemother.* **51**, 4205–4208 (2007).
468 32. Huseby, D. L. *et al.* Mutation supply and relative fitness shape the genotypes of
469 ciprofloxacin-resistant *Escherichia coli*. *Mol. Biol. Evol.* **34**, 1029–1039 (2017).
470 33. Zhao, S. *et al.* Adaptive Evolution within Gut Microbiomes of Healthy People. *Cell Host*
471 *Microbe* **25**, 656-667.e8 (2019).
472 34. Poyet, M. *et al.* A library of human gut bacterial isolates paired with longitudinal multiomics
473 data enables mechanistic microbiome research. *Nat. Med.* **25**, 1442–1452 (2019).
474 35. Garud, N. R., Good, B. H., Hallatschek, O. & Pollard, K. S. Evolutionary dynamics of bacteria
475 in the gut microbiome within and across hosts. *PLoS Biol.* **17**, e3000102 (2019).

476 36. Yaffe, E. & Relman, D. A. Tracking microbial evolution in the human gut using Hi-C reveals
477 extensive horizontal gene transfer, persistence and adaptation. *Nat. Microbiol.* **5**, 343–353
478 (2020).
479 37. Roodgar, M. *et al.* Longitudinal linked-read sequencing reveals ecological and evolutionary
480 responses of a human gut microbiome during antibiotic treatment. *Genome Res.* **31**, 1433–
481 1446 (2021).
482 38. Zlitni, S. *et al.* Strain-resolved microbiome sequencing reveals mobile elements that drive
483 bacterial competition on a clinical timescale. *Genome Med.* **12**, 50 (2020).
484 39. Chen, D. W. & Garud, N. R. Rapid evolution and strain turnover in the infant gut
485 microbiome. *Genome Res.* **32**, 1124–1136 (2022).
486 40. Pecquet, S., Ravoire, S. & Andremont, A. Faecal excretion of ciprofloxacin after a single oral
487 dose and its effect on faecal bacteria in healthy volunteers. *J. Antimicrob. Chemother.* **26**,
488 125–129 (1990).
489 41. Fantin, B. *et al.* Ciprofloxacin Dosage and Emergence of Resistance in Human Commensal
490 Bacteria. *J. Infect. Dis.* **200**, 390–398 (2009).
491 42. Dethlefsen, L. & Relman, D. A. Incomplete recovery and individualized responses of the
492 human distal gut microbiota to repeated antibiotic perturbation. *Proc. Natl. Acad. Sci.* **108**,
493 4554–4561 (2011).
494 43. Truong, D. T., Tett, A., Pasolli, E., Huttenhower, C. & Segata, N. Microbial strain-level
495 population structure and genetic diversity from metagenomes. *Genome Res.* **27**, 626–638
496 (2017).
497 44. MetaHIT Consortium *et al.* Identification and assembly of genomes and genetic elements in
498 complex metagenomic samples without using reference genomes. *Nat. Biotechnol.* **32**, 822–
499 828 (2014).
500 45. Nayfach, S., Shi, Z. J., Seshadri, R., Pollard, K. S. & Kyrpides, N. C. New insights from
501 uncultivated genomes of the global human gut microbiome. *Nature* **568**, 505–510 (2019).
502 46. Nissen, J. N. *et al.* Improved metagenome binning and assembly using deep variational
503 autoencoders. *Nat. Biotechnol.* **39**, 555–560 (2021).
504 47. Quince, C. *et al.* DESMAN: a new tool for de novo extraction of strains from metagenomes.
505 *Genome Biol.* **18**, 181 (2017).
506 48. Smillie, C. S. *et al.* Strain Tracking Reveals the Determinants of Bacterial Engraftment in the
507 Human Gut Following Fecal Microbiota Transplantation. *Cell Host Microbe* **23**, 229-240.e5
508 (2018).
509 49. Quince, C. *et al.* STRONG: metagenomics strain resolution on assembly graphs. *Genome
510 Biol.* **22**, 214 (2021).
511 50. Good, B. H. & Desai, M. M. Deleterious Passengers in Adapting Populations. *Genetics* **198**,
512 1183–1208 (2014).
513 51. Orillard, E. & Tan, M. Functional analysis of three topoisomerases that regulate DNA
514 supercoiling levels in *Chlamydia*. *Mol. Microbiol.* **99**, 484–496 (2016).
515 52. Hirsch, J. & Klostermeier, D. What makes a type IIA topoisomerase a gyrase or a Topo IV?
516 *Nucleic Acids Res.* **49**, 6027–6042 (2021).
517 53. Helgesen, E., Sætre, F. & Skarstad, K. Topoisomerase IV tracks behind the replication fork
518 and the SeqA complex during DNA replication in Escherichia coli. *Sci. Rep.* **11**, 474 (2021).

519 54. Zhao, X. *et al.* Lethal Action of Quinolones against a Temperature-Sensitive *dnaB* Replication
520 Mutant of *Escherichia coli*. *Antimicrob. Agents Chemother.* **50**, 362–364 (2006).
521 55. Rubin, D. H., Mortimer, T. D. & Grad, Y. H. Neisseria gonorrhoeae diagnostic escape from a
522 gyrA-based test for ciprofloxacin susceptibility and the effect on zoliflodacin resistance: a
523 bacterial genetics and experimental evolution study. *Lancet Microbe* **4**, e247–e254 (2023).
524 56. Ghosh, O. M. & Good, B. H. Emergent evolutionary forces in spatial models of luminal
525 growth and their application to the human gut microbiota. *Proc. Natl. Acad. Sci.* **119**,
526 e2114931119 (2022).
527 57. Kent, A. G., Vill, A. C., Shi, Q., Satlin, M. J. & Brito, I. L. Widespread transfer of mobile
528 antibiotic resistance genes within individual gut microbiomes revealed through bacterial Hi-
529 C. *Nat. Commun.* **11**, 4379 (2020).
530 58. Bishara, A. *et al.* High-quality genome sequences of uncultured microbes by assembly of
531 read clouds. *Nat. Biotechnol.* **36**, 1067–1075 (2018).
532 59. Suzuki, Y. *et al.* Long-read metagenomic exploration of extrachromosomal mobile genetic
533 elements in the human gut. *Microbiome* **7**, 119 (2019).
534 60. Moss, E. L., Maghini, D. G. & Bhatt, A. S. Complete, closed bacterial genomes from
535 microbiomes using nanopore sequencing. *Nat. Biotechnol.* **38**, 701–707 (2020).
536 61. Croucher, N. J. *et al.* Evidence for Soft Selective Sweeps in the Evolution of Pneumococcal
537 Multidrug Resistance and Vaccine Escape. *Genome Biol. Evol.* **6**, 1589–1602 (2014).
538 62. Andersson, D. I. & Hughes, D. Antibiotic resistance and its cost: is it possible to reverse
539 resistance? *Nat. Rev. Microbiol.* **8**, 260–271 (2010).
540 63. Marcusson, L. L., Frimodt-Møller, N. & Hughes, D. Interplay in the Selection of
541 Fluoroquinolone Resistance and Bacterial Fitness. *PLoS Pathog.* **5**, e1000541 (2009).
542 64. Yao, H. *et al.* Emergence of a Potent Multidrug Efflux Pump Variant That Enhances
543 *Campylobacter* Resistance to Multiple Antibiotics. *mBio* **7**, e01543-16 (2016).
544 65. Baker, S. *et al.* Fitness benefits in fluoroquinolone-resistant *Salmonella* Typhi in the absence
545 of antimicrobial pressure. *eLife* **2**, e01229 (2013).
546 66. Sommer, M. O. A., Munck, C., Toft-Kehler, R. V. & Andersson, D. I. Prediction of antibiotic
547 resistance: time for a new preclinical paradigm? *Nat. Rev. Microbiol.* **15**, 689–696 (2017).
548 67. Bolger, A. M., Lohse, M. & Usadel, B. Trimmomatic: a flexible trimmer for Illumina sequence
549 data. *Bioinformatics* **30**, 2114–2120 (2014).
550 68. Schmieder, R. & Edwards, R. Fast Identification and Removal of Sequence Contamination
551 from Genomic and Metagenomic Datasets. *PLoS ONE* **6**, e17288 (2011).
552 69. Li, D., Liu, C. M., Luo, R., Sadakane, K. & Lam, T. W. MEGAHIT: An ultra-fast single-node
553 solution for large and complex metagenomics assembly via succinct de Bruijn graph.
554 *Bioinformatics* **31**, 1674–1676 (2014).
555 70. Li, H. & Durbin, R. Fast and accurate short read alignment with Burrows-Wheeler transform.
556 *Bioinforma. Oxf. Engl.* **25**, 1754–1760 (2009).
557 71. Kang, D. D. *et al.* MetaBAT 2: an adaptive binning algorithm for robust and efficient genome
558 reconstruction from metagenome assemblies. *PeerJ* **7**, e7359 (2019).
559 72. Mende, D. R. *et al.* proGenomes2: an improved database for accurate and consistent
560 habitat, taxonomic and functional annotations of prokaryotic genomes. *Nucleic Acids Res.*
561 **48**, D621–D625 (2019).

562 73. Parks, D. H., Imelfort, M., Skennerton, C. T., Hugenholtz, P. & Tyson, G. W. CheckM:
563 assessing the quality of microbial genomes recovered from isolates, single cells, and
564 metagenomes. *Genome Res.* **25**, 1043–1055 (2015).
565 74. Chaumeil, P.-A., Mussig, A. J., Hugenholtz, P. & Parks, D. H. GTDB-Tk v2: memory friendly
566 classification with the genome taxonomy database. *Bioinformatics* **38**, 5315–5316 (2022).
567 75. Schliep, K. P. phangorn: phylogenetic analysis in R. *Bioinformatics* **27**, 592–593 (2011).
568 76. Hyatt, D. *et al.* Prodigal: prokaryotic gene recognition and translation initiation site
569 identification. *BMC Bioinformatics* **11**, 119 (2010).
570 77. Buchfink, B., Xie, C. & Huson, D. H. Fast and sensitive protein alignment using DIAMOND.
571 *Nat. Methods* **12**, 59–60 (2015).
572 78. Steinegger, M. & Söding, J. MMseqs2 enables sensitive protein sequence searching for the
573 analysis of massive data sets. *Nat. Biotechnol.* **35**, 1026–1028 (2017).
574 79. Huerta-Cepas, J. *et al.* eggNOG 5.0: a hierarchical, functionally and phylogenetically
575 annotated orthology resource based on 5090 organisms and 2502 viruses. *Nucleic Acids*
576 *Res.* **47**, D309–D314 (2019).
577 80. Sievers, F. *et al.* Fast, scalable generation of high-quality protein multiple sequence
578 alignments using Clustal Omega. *Mol. Syst. Biol.* **7**, 539 (2011).
579 81. Hartl, D. L. & Clark, A. G. *Principles of population genetics*. (Sinauer Associates, 2007).
580 82. Gillespie, J.H. *Population Genetics: A Concise Guide.* (Johns Hopkins University Press, 2004).

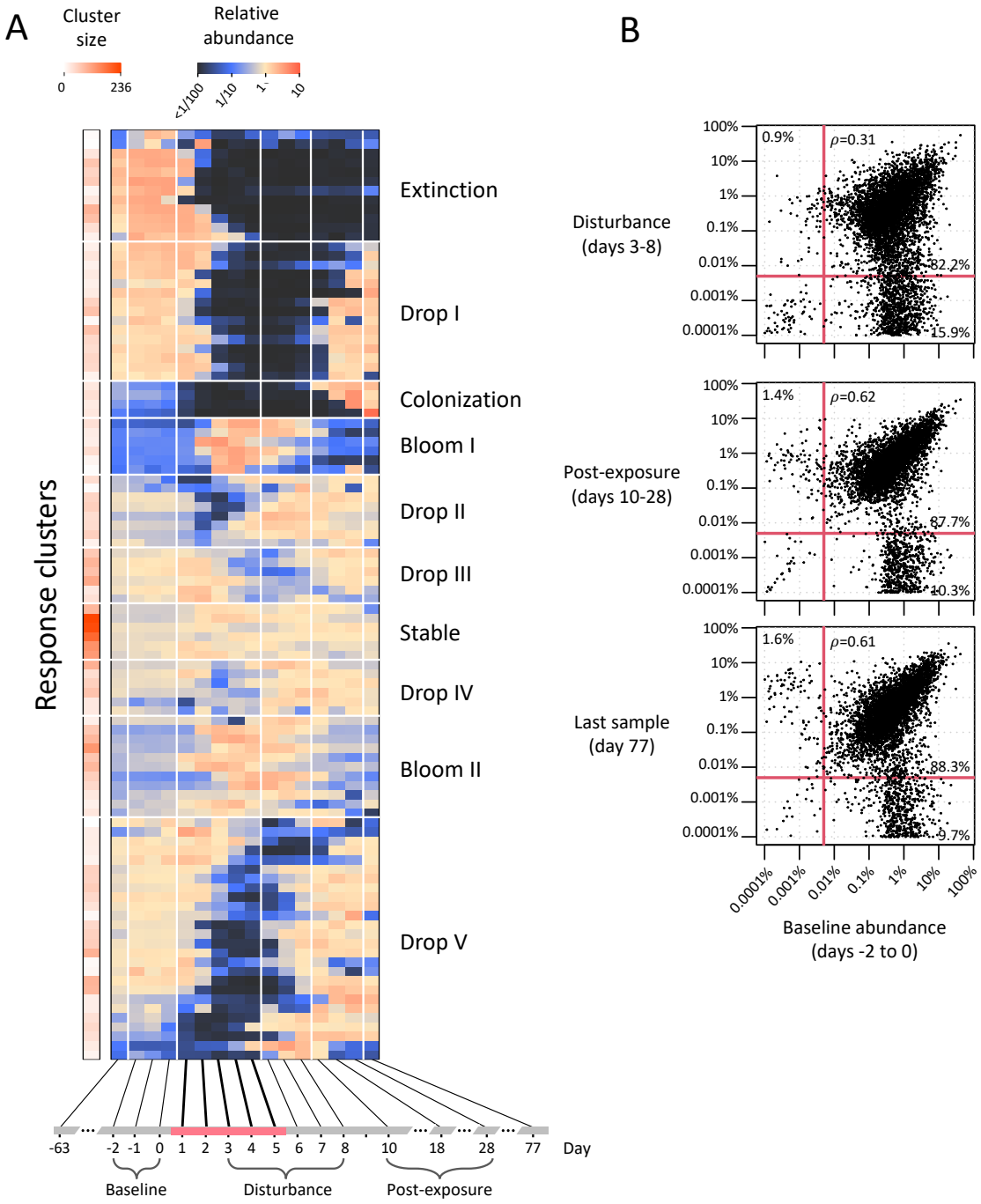

Fig. 1. Population-level responses to ciprofloxacin. A) Abundance trajectories of all 5665 metagenome-assembled genomes (MAGs) were each normalized relative to their respective mean and clustered using k-means into 100 response clusters or trends. Trends are organized vertically using hierarchical clustering, with the number of populations per cluster shown by a color bar on the left. The mean-centered abundance of each cluster across 16 temporal samples is shown horizontally, with ciprofloxacin course days indicated in red along the axis (shifted by a day to reflect transit time). **B)** Scatter plots comparing the baseline pre-exposure population

abundances to three later timeframes. Each scatter plot depicts for each population the baseline abundance (x-axis, average of days -2 to 0) vs. one of three timeframes (during the height of disturbance at days 3-8, post exposure at days 10-28, and on the last day of sampling, day 77). A pseudo-count of 0.0001% was added to each count for visualization purposes. Vertical/horizontal red lines represent a detection threshold of 0.005%. The percentages of populations within quadrants are shown, as are Spearman correlation coefficients between populations detected in both timeframes.

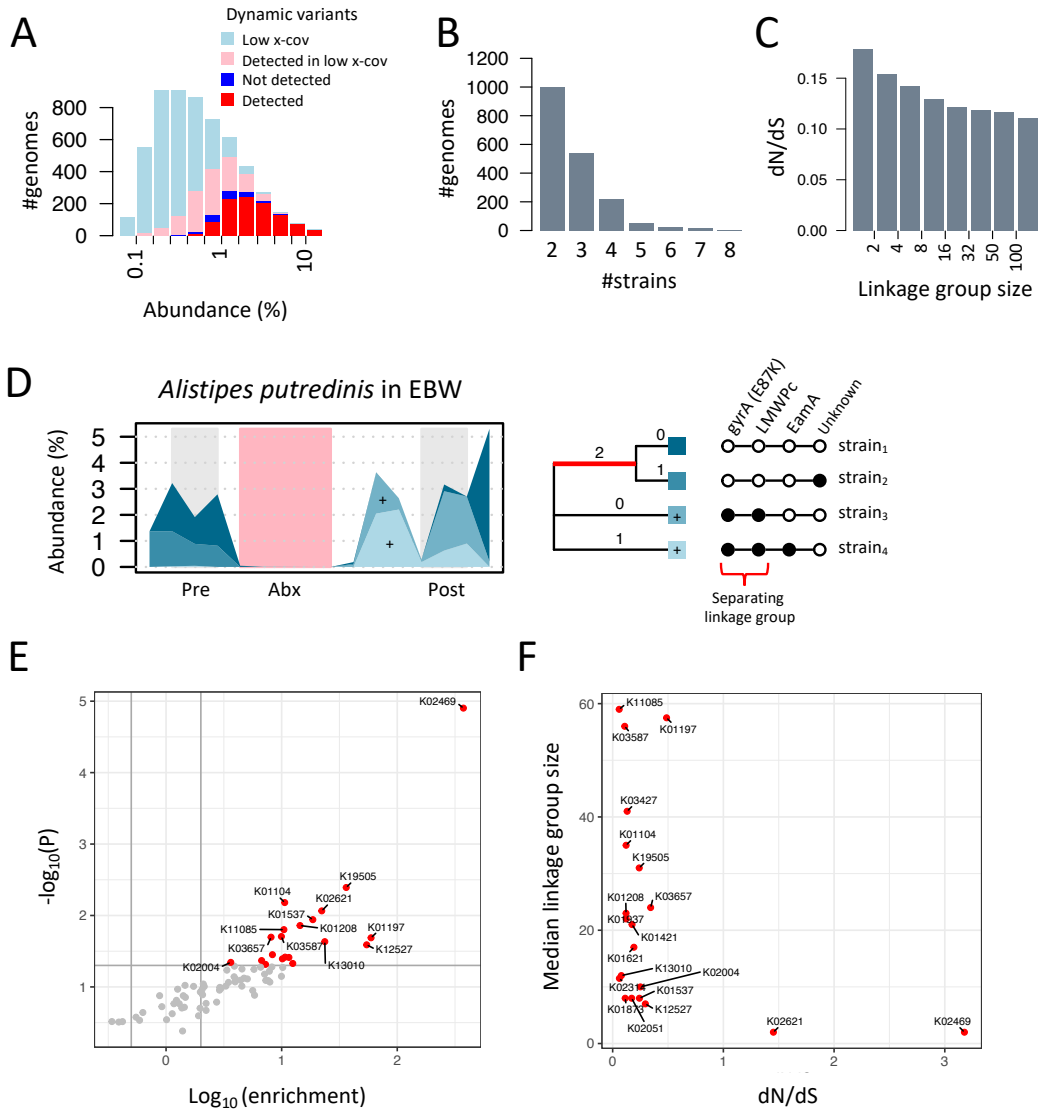

Fig 2. Variants, strains, linkage groups and converging evolution analysis. A) Number of population genomes (y-axis) as a function of the average population abundance (x-axis). Colors denote four population types: 1018 populations with dynamic variants and sufficient x-coverage to detect sweeps if present (red, "Detected"), 168 populations with no dynamic variants and sufficient x-coverage (dark blue, "Not detected"), 1115 populations with dynamic variants and low x-coverage (pink, "Detected in low x-cov"), and 3364 populations with no variants and low x-coverage (light blue, "Low x-cov"). **B)** Number of genomes containing dynamic variants (y-axis) as a function of the number of inferred strains (x-axis). **C)** dN/dS ratios (y-axis) as a function of the linkage group (LG) size (x-axis). **D)** Temporal dynamics of the population of *Alistipes putredinis* in subject EBW. On the right is the variant-strain matrix, with 4 bi-allelic polymorphic loci (columns, named according to gene), and 4 strains (rows), with black and white circles depicting

the variants present in a strain. The strain phylogeny (generated through maximum parsimony) is shown in the middle, with the number of switching variants displayed above each edge. The edge associated with the linkage group that separates strains 1+2 from strains 3+4 is colored in red. Shown on the left is the temporal abundance of strains (strains stacked) over the 16 temporal samples (x-axis), with background colors emphasizing pre (antibiotic) samples (days -2 to 0, gray), disturbed samples (days 3-8, pink) and post (antibiotic) samples (days 10-28, gray). Plus signs denote strains 3 and 4, which become the dominant strains after the exposure. Strain order and representation as shades of blue are consistent across the panel. **E)** Variants were assigned weights equal to the inverse of their smallest linkage group, weights were aggregated within KEGG Orthology annotations (KOs) of associated genes and then compared to a null model of weights across KOs generated through permutations. A volcano plot depicts weight enrichment ratios over the null model (x-axis) vs. P-values (y-axis). Significant KOs ($P<0.05$) are colored red. K02469 is *gyrA* and K02621 is *parC*, other KO descriptions are given in **Supp. Figure S12**. **F)** For each significant KO, the dN/dS ratio (x-axis) of the supporting variants is plotted vs. the median linkage group size of the supporting variants (y-axis).

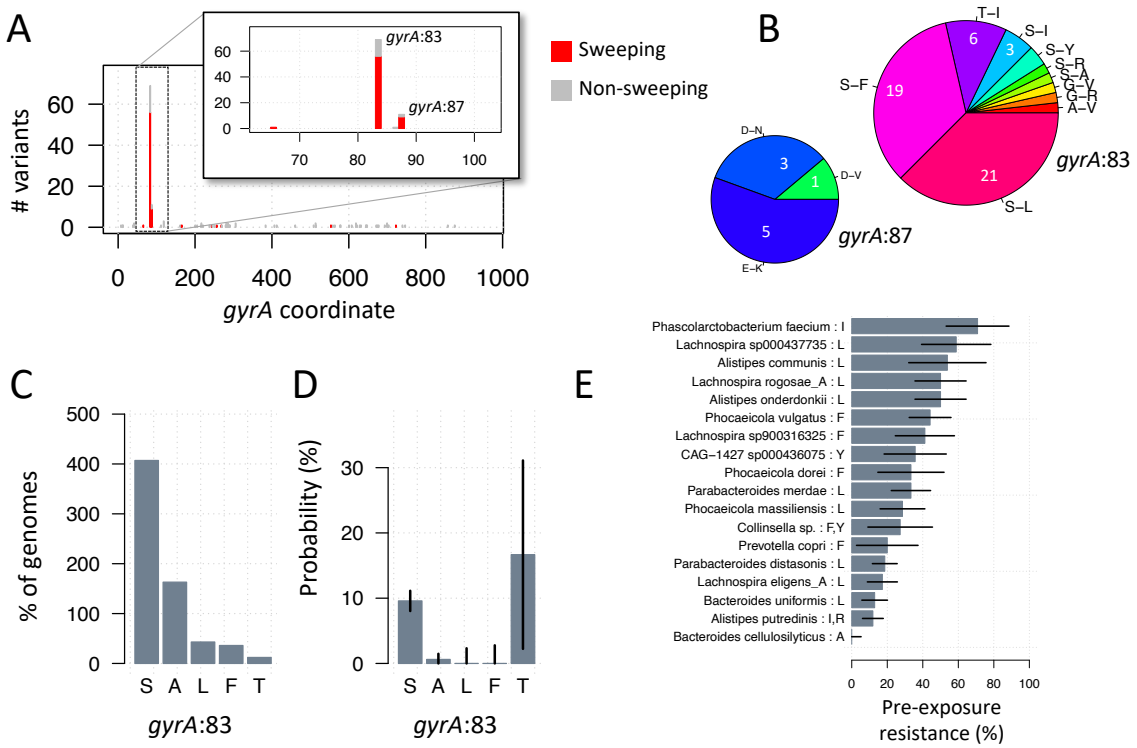

Fig. 3. Focused selective pressure on *gyrA*. A) The number of variants (y-axis) for each amino acid (AA) position within the *gyrA* gene (x-axis, *E. coli* numbering). Sweeping and non-sweeping variant counts are colored red and gray respectively. **B)** Breakdown of substitutions associated with sweeping variants at *gyrA*:83 and *gyrA*:87, letters represent amino acids (e.g., 'S-F' represents a substitution of serine by phenylalanine). **C)** Breakdown of all genomes containing *gyrA* according to the baseline AA identity at *gyrA*:83 before the exposure. **D)** Exposure-associated substitution probability, stratified by the baseline AA at *gyrA*:83. Confidence intervals showing the standard deviation depicted with vertical lines. **E)** Species-specific resistance alleles at *gyrA*:83 were determined for 31 species based on observed exposure-associated substitutions. The percentage of resistance alleles prior to exposure is shown for 18 species represented by at least 10 populations. Resistance alleles are shown next to the species name. For example, *Alistipes putredinis* has two resistance alleles at *gyrA*:83, namely isoleucine ('I') and arginine ('R'), and 12% (5/42) of *A. putredinis* populations had either of these alleles prior to the exposure. Black bars represent standard deviation estimates.

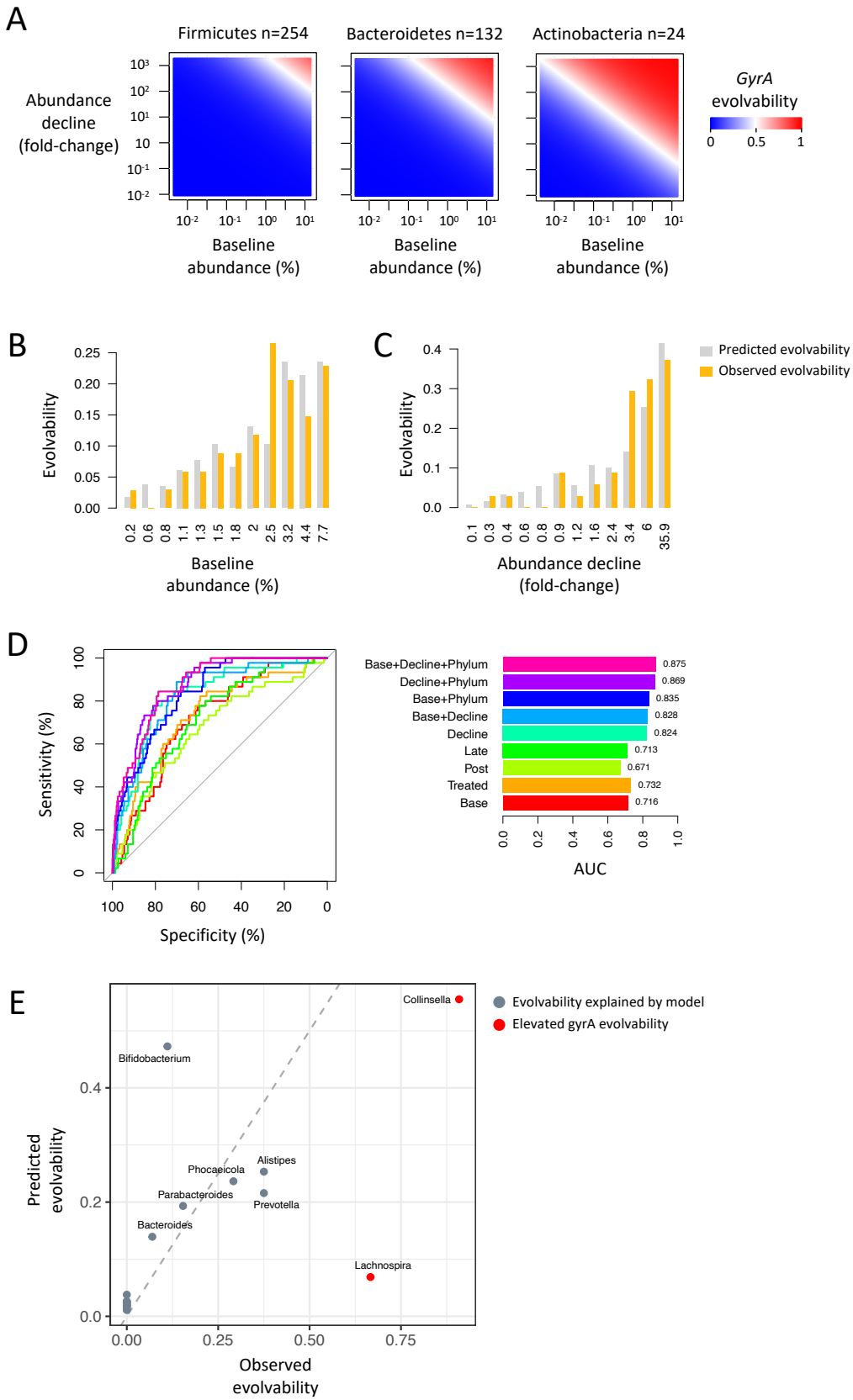
A
Firmicutes n=254
Bacteroidetes n=132
Actinobacteria n=24
Abundance decline (fold-change)
Baseline abundance (%)
GyrA evolvability
B
Evolvability
Baseline abundance (%)
C
Evolvability
Abundance decline (fold-change)
Predicted evolvability
Observed evolvability
D
Sensitivity (%)
Specificity (%)
Base+Decline+Phylum 0.875
Decline+Phylum 0.869
Base+Phylum 0.835
Base+Decline 0.828
Decline 0.824
Late 0.713
Post 0.671
Treated 0.732
Base 0.716
AUC
E
Collinsella
Bifidobacterium
Phocaeicola
Alistipes
Parabacteroides
Prevotella
Bacteroides
Lachnospira
Predicted evolvability
Observed evolvability
Evolvability explained by model
Elevated gyrA evolvability

Fig. 4. Abundance-dependent evolution of antibiotic resistance. A) *GyrA* evolvability as predicted by a fitted logistic regression model based on variables for the baseline population abundance (average of days -2 to 0, x-axis), the fold-change decline during antibiotics (average of days 1-5, y-axis), and phylum (separate plot for each of three phyla). **B)** Model-predicted and observed *gyrA* evolvability (y-axis) as a function of baseline abundances. **C)** Model-predicted and observed *gyrA* evolvability (y-axis) as a function of the fold-change decline in population abundances during antibiotics (days 1-5). **D)** Shown on left are ROC curves (receiver operating characteristic curves) of 9 inferred logistic regression models that predict the probability of a population to have a sweeping *gyrA* variant. Shown on right are the areas under the curve (AUC) of all models. **E)** Observed (x-axis) vs. model-predicted (y-axis) genus-level *gyrA* evolvability, for the 21 genera associated with at least 6 populations. Genera are colored red if differences between observed and predicted evolvability were significant (Binomial distribution, $P<0.05$), and colored gray otherwise. Dashed line depicts the line x=y.

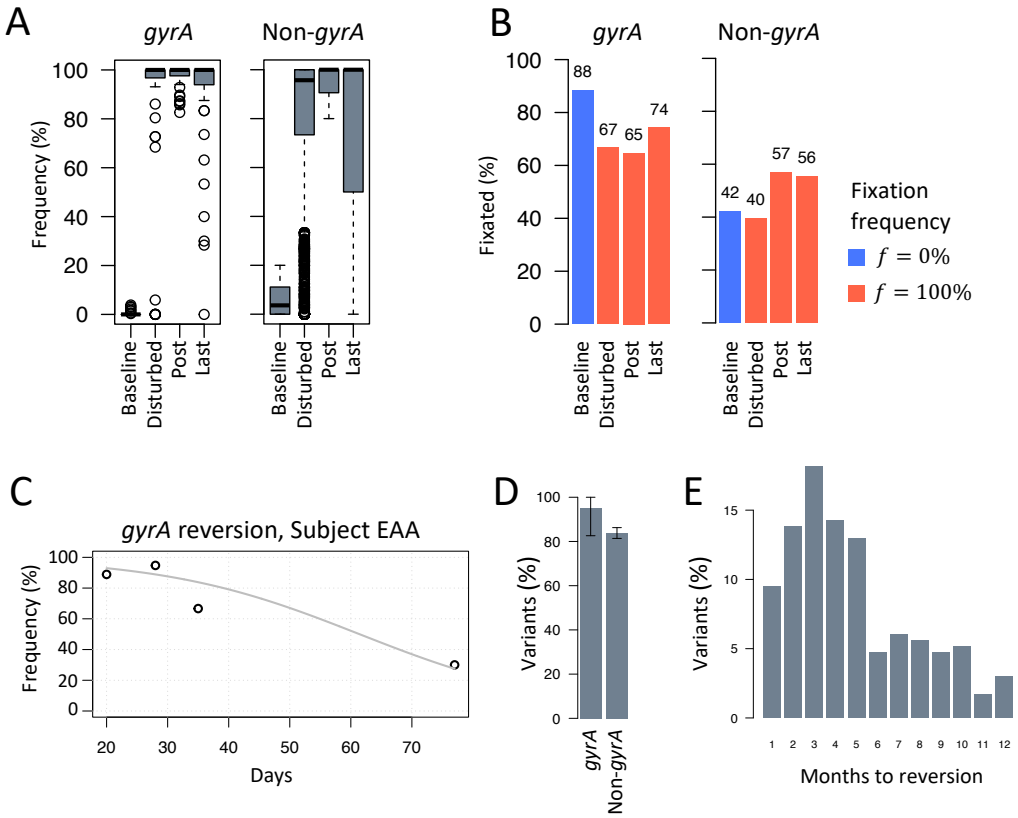

Fig. 5. Long-term persistence of antibiotic-associated genetic changes. A) Boxplots depicting the distribution of the frequencies of sweeping *gyrA* variants (left) and non-*gyrA* variants (right), stratified by time windows (day ranges defined in panel 1A). Gray rectangles span the first and third quartiles, horizontal line depicts the median, dashed line spans between the 5th and the 95th percentiles, and outliers outside that range are plotted as circles. **B)** The percentage of sweeping variants fixated at 0% frequency at baseline (blue) or fixated at 100% within the 3 other time windows (red), shown separately for *gyrA* variants (left) and non-*gyrA* variants (right). **C)** Example of a sweeping *gyrA* variant in subject EAA that was projected to revert below a frequency of 1% within 135 days. Circles depict the variant frequency (y-axis) as a function of the day relative to the start of the antibiotics (x-axis). Gray line shows an exponential decay, based on a constant selection coefficient of 0.006 that was inferred from the temporal frequency data, assuming 10 generations per day. **D)** The percentage of sweeping *gyrA* variants (left) and sweeping non-*gyrA* variants (right) that were projected to require more than a year to revert below a frequency of 1%. Vertical lines depict estimates of the standard deviation. **E)** For sweeping variants that were projected to fall below a frequency of 1% within a year, a histogram of the number of months until reversion.